DOI 10.5162/sensor2015/C5.3

# Sonographic Detection of Nanoparticles used for Magnetic Drug Targeting

Michael Fink[1*], Helmut Ermert[1], Michael Löffler[1], Alexander Sutor[1], Barbara Tewes[1], Andreas Koch[1], Christoph Alexiou[2], Stefan Lyer[2]
[1] Chair of Sensor Technology, Friedrich-Alexander-Universität Erlangen-Nürnberg (FAU), Germany, *michael.fink@fau.de
[2] Section for Experimental Oncology and Nanomedicine (SEON), University Hospital Erlangen, Germany

**Abstract:**
The aim of magnetic drug targeting (MDT) in cancer therapy is to locally increase chemotherapeutic agent density in the area of cancerous tissue. For this purpose, chemotherapeutic drugs are bound to superparamagnetic iron oxide nanoparticles, stabilized by a biocompatible layer. This compound then can be applied intra-arterially in the vicinity of a tumor. With the aid of an external, static magnetic field or rather a magnetic field gradient an accumulation of the nanoparticles and thus the drug in the region of interest is achieved [1]. Due to the lack of specificity of chemotherapeutic drugs for tumor cells, in conventional cancer treatment, a high dosage has to be applied to reach a sufficient concentration in the tumor area. This usually results in serious side effects in patients. The advantage of MDT is to obtain a higher dose of drug in the tumor region, while the overall dose and thereby side effects are reduced [2]. As accumulation of nanoparticles in the appropriate region is of vital importance for MDT, one should be able to visualize the particle concentration in the tissue. However, nanoparticles are not visible directly because of their weak backscattering using ultrasound imaging techniques. In this paper, we present a possibility to visualize these nanoparticles. It is based on exciting a periodic motion of the nanoparticles using an external, time harmonic magnetic field. The particles force the surrounding tissue to move also, and this can be visualized by ultrasound imaging techniques. Three different evaluation algorithms are investigated in this contribution.

**Key words:** Magnetic Drug Targeting, superparamagnetic nanoparticles, ultrasound imaging, magnetic force

## Introduction

The presence of magnetic nanoparticles in cancerous biological tissue is of vital importance in Magnetic Drug Targeting (MDT), a new cancer treatment technique. These superparamagnetic nanoparticles (SPIONs) are used as carriers for chemotherapeutic drugs. The SPIONs are injected intra-arterially in the vicinity of a tumor and accumulated by a strong external magnetic field in the tumor area [1]. In the to date biggest preclinical animal study for MDT an already very high efficiency could be shown, recently [6]. In the therapy arm of this study, performed by using a VX2 subcutaneous tumor model, 30% of the rabbits could be cured after one single administration of only 5% or 10% of a single dose of mitoxantron. The biodistribution showed that more than 50% of the drug that could be found again after 24 hours was located in the tumor region. Another possibility offered by SPIONs is to be able to distinguish particle loaded tissue from tissue which is free of particles by using distinct magnetic properties of the nanoparticles. This could be used for estimating the amount of nanoparticles deposited in the tumor area and by that the amount of the bound drug, too. One option for this is MRI. It is known, that magnetic nanoparticles are causing a signal extinction in the tissue, where they are deposited and this can be of high diagnostic value [7, 8]. Another option could be magnetic particle imaging (MPI). For this new imaging technique, SPIONs are used as contrast agents [9]. MRI is commonly used in clinics as standard imaging technique and MPI is still in development, but both techniques have in common, that they need relatively large technical equipment and are very cost intensive.

On the other hand, ultrasound, a widespread imaging technique with rather low costs and a high flexibility, could also be used for imaging tissue that has incorporated magnetic nanoparticles. For this purpose, a periodic motion of the nanoparticles is excited using an

external, time harmonic magnetic field $\vec{B}(\vec{r},t)$. The magnetic force $\vec{F}(\vec{r},t)$ on nanoparticles can be calculated [3] by

$$\vec{F}(\vec{r},t) = \chi_S \cdot V \cdot \nabla \left( \frac{\left|\vec{B}(\vec{r},t)\right|^2}{2\mu_0} \right). \qquad (1)$$

The magnetic force depends on the spatial position $\vec{r}$, the susceptibility $\chi_S$ of the nanoparticle material, the volume $V$ of the nanoparticles and on the magnetic field gradient at the place, where the particles are located. The latter one is an external impact factor and should be chosen as large as possible to achieve a large measuring effect. The volume of the particles is determined by the application, whereby the radius should not exceed 200 nm to be suitable for sterile filtration and to prevent occlusion of vessels. Due to the core size, the nanoparticles used in this work have superparamagnetic properties, which means that there is no hysteretic behavior observable. The external time harmonic magnetic field leads to motions of the nanoparticles and consequently to a vibration of the surrounding tissue, too. This tissue movement can be visualized by ultrasound imaging techniques. The evaluation algorithms are based on the magnetically-evoked, harmonic vibration of the tissue with twice the frequency $f_0$ of the alternating magnetic field [3]. With a view to identifying the vibrating regions of tissue, a sequence of ultrasound images has to be recorded. In Method A, the Fourier Transform of the time-discrete echo signal of each pixel of the image is computed and evaluated at the expected frequency of motion. Method B is based on 2-dimensional template matching. Here, the movement of a snippet of the sonogram across the single images of the sequence is monitored and transformed into frequency domain. In the 2-dimensional case the evaluation algorithm is carried out on the basis of the gray-scaled images. Method C employes 1-dimensional template matching. In contrast to Method B, the received high frequency ultrasound signals rather than the merged gray-scale images are analyzed. All investigations were performed with tissue mimicking phantoms. The composition and production of these phantoms as well as the experimental setup are presented in the following sections. Finally the three different evaluation algorithms to detect magnetic nanoparticles are described and compared.

**Materials**

In order to produce a phantom, tissue mimicking material was made out of PVA (Polyvinyl alcohol). The PVA was dissolved in water at a temperature of 90°C, where the rate of PVA was 10% by weight. After cooling down the obtained material to a temperature of 60°C, a 10 mm diameter silicone bubble containing magnetic nanoparticles was surrounded by the tissue mimicking material. The phantom then went through two freeze-thaw cycles, whereby each cycle lasted 30 hours (15 hours freeze, 15 hours thaw). The processing conditions of the freeze-thaw cycles and the number of repetitions of the freeze-thaw cycles are of essential importance for the final mechanical and therefore acoustic properties [4].

The superparamagnetic nanoparticles were produced at the the Section of Experimental Oncology and Nanomedicine (SEON), University Hospital Erlangen, Germany. The particles consist of a 5 – 20 nm diameter iron oxide core, surrounded by a lauric acid layer. The outer layer prevents agglomeration of the particles. The hydrodynamic diameter of a whole particle is about 30 – 200 nm [5].

**Experimental Setup**

All measurements were performed with the ultrasound system ACUSON Antares (Siemens). A VFX 13-5 (Siemens) linear array was used as ultrasound transducer. In order to detect vibrations in the observed tissue, a sequence of ultrasound images was recorded, whereby the framerate was chosen to be 109 frames per second (overall 373 frames), which meant a recording time of $t_{tot}$ = 3,42 s. The ultrasonic center frequency was 10 MHz and the B-mode images had a size of 140 (lateral) x 1972 (axial) pixels. The measurement setup can be seen in Fig. 1.

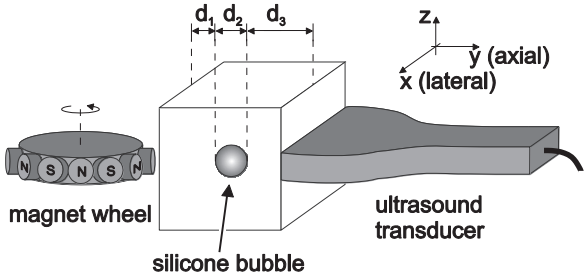


*Fig. 1. Experimental setup.*

A magnet wheel was used to induce an alternating magnetic field. The magnet wheel consists of a round iron core with 12 cylindrical NdFeB magnets (9 mm diameter, 5 mm length, magnetized along the main axis) on the edge. Figure 2 shows the magnetic flux density of one of these magnets as a function of the distance

to the magnet surface. As can be seen from Fig. 2, an increasing distance to the magnet leads to a decreasing magnetic field gradient.

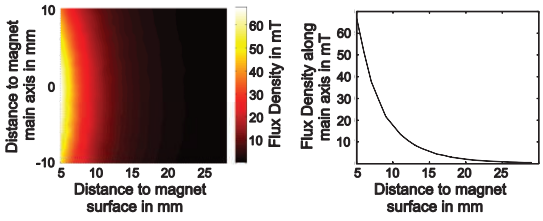


*Fig. 2. Flux density resulting from a cylindrical NdFeB magnet (9 mm diameter, 5 mm length).*

The magnet should therefore be as close as possible to the particle loaded tissue. The magnet wheel was rotated by a DC electric motor so that the frequency of the alternating magnetic field was $f_0$ = 10 Hz. The phantom was positioned between the ultrasound transducer and the magnet wheel, whereby the distance between the magnet wheel and the silicone bubble was $d_1$ = 5 mm. The distance between the ultrasound transducer and the bubble was $d_3$ = 35 mm. The collected radio frequency (RF) data were exported to Matlab R2013b (MathWorks Inc.) and were postprocessed using three different evaluation algorithms.

## Method A

Method A is based on calculating the amplitude spectrum of the received RF data. The variation of the amplitude of the collected high frequency signals is observed over time at each pixel of the B-mode image. Figure 3 illustrates the evaluation principle according to Method A. The alternating magnetic field at the frequency $f_0$ leads to an oscillation of the magnetic nanoparticles at $2f_0$.

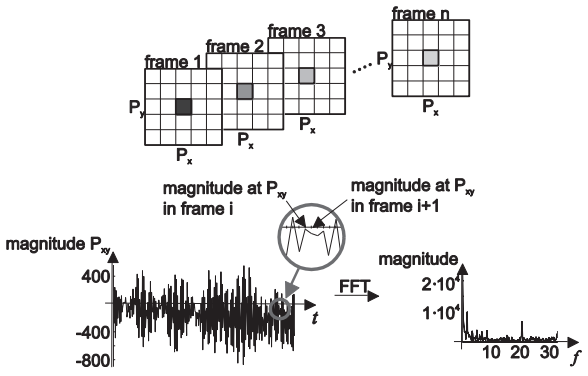


*Fig. 3. Method A: FFT of the magnitude of the RF data at a certain pixel $P_{xy}$ (60, 1600) observed over all frames.*

Because of their weak backscattering, the superparamagnetic nanoparticles are not detectable by means of conventional ultrasound imaging techniques. However, particle movement also leads to tissue movement in the vicinity of the particles, which offers a measurable effect. The content of the silicone bubble consists of nanoparticles dissolved in water, which results in weak backscattering. Thus, the particle solution of the silicone bubble cannot be made visible by employing this measurement technique. However, the oscillation of the nanoparticles at the frequency $2f_0$ leads to an oscillation of the whole silicone bubble itself at the same frequency. This movement of the silicone bubble can be visualized by means of ultrasound imaging techniques by the detection of the bubble wall echoes. In a first step, the magnitude values at a certain pixel $P_{xy}$ is observed over all frames. In a second step, the Fast Fourier Transform of this chart is calculated whereat only the magnitude spectrum is of interest. In case of any tissue movement resulting from the particle oscillation a corresponding $2f_0$ component should occur in the FT.

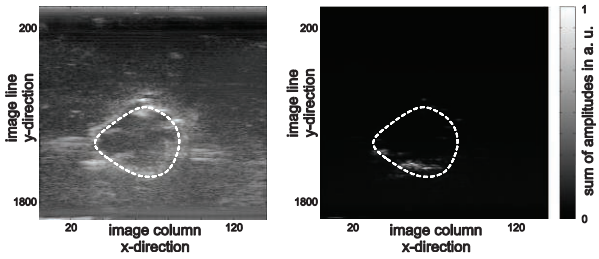


*Fig. 4. Ultrasound B-mode image of silicone bubble containing iron oxide nanoparticles (left) and tissue movement with twice the frequency of the alternating magnetic field using Method A (right). The edge of the bubble is indicated by the dashed line.*

Since the exciting magnetic field may slightly differ from 10 Hz, all signals in the range 20 ± 1 Hz are considered. The values in this frequency band are summed up. The result of this summation can be seen as an indicator of the presence of magnetically induced particle movement. This approach is applied to each pixel. Figure 4 illustrates the results using the algorithm according to Method A. As one can see, movements of the bubble can be found in the appropriate frequency band. Especially in the lower part of the image movements with the frequency $2f_0$ can be detected. This results from the position of the magnet wheel, which is located at the bottom of the picture. Thus, the magnetic flux density and also the magnetic field gradient decrease from the bottom to the top of the picture. According to equation (1), the magnetic force and therefore the strength of the measuring effect decrease from bottom to top. The advantage of Method A is that the evaluation is based on the RF data, which means no loss of information. Furthermore, this

algorithm is characterized by a short calculation time. A disadvantage of this algorithm is that the direction of the particle movement is not taken into account. It can be assumed, however, that only the direction along the image lines (y-direction), which is parallel to the direction of the magnetic field gradient, is of relevance. Particle movement along the image column direction (x-direction) can be neglected.

**Method B**

Method B is based on a 2-dimensional cross-correlation. The bubble movement at the frequency $2f_0$ leads to a variation of the gray-scaled values of the B-mode image. In order to detect the shift of a certain section of the B-mode image from one frame to another, the interesting section is cut out of the frame. Figure 5 illustrates the evaluation principle according to Method B. The pixel $P_{xy}$ is located in the center of the separated template. Afterwards the template is searched in the second frame and the shift in x- and y-direction is identified. In another step the template is also searched in the other frames while for each frame the shift in x- and y- direction is identified. Afterwards, the time dependent behavior of the template shift in x- and y-direction is Fourier transformed. Similar to Method A the values of the frequency band $2f_0 \pm 1$ Hz are summed up. The movement direction results from the absolute value of the movement in x- and y-direction. A disadvantage of Method B is that the algorithm is based on the gray-scaled B-mode images. The transition from RF data to the gray-scaled image implies a loss of information.

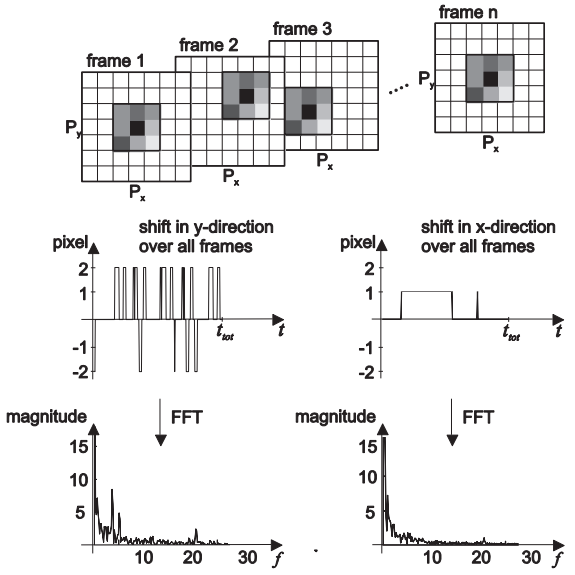


*Fig. 5. Method B: 2D Template Matching (center pixel of template $P_{xy}$ (60, 1600)).*

Another disadvantage using this evaluation algorithm is that because of the cross-correlation, calculation time is larger than using Method A. This disadvantage can be minimized reducing the size of the templates as well as reducing the area in which the template is searched in the other frames. The problem here is that the position of the template in the other frames is unknown. It can be assumed, however, that the shift from one frame to another is very small. As can be seen in Fig. 5, the shift is in the range of -2 to +2 pixels. Figure 6 shows the results using the algorithm according to Method B. One can see from Fig. 6 that tissue movement in the appropriate region can be detected. As discussed at Method A the measuring effect is only usable at the bottom of the silicone bubble, which is the region close to the magnet wheel. Tissue movement in the appropriate frequency band also seems to occur in the top region of the resulting image. As the original B-mode image does not contain any echo-signals from that area, it can be assumed that these signals represent noise.

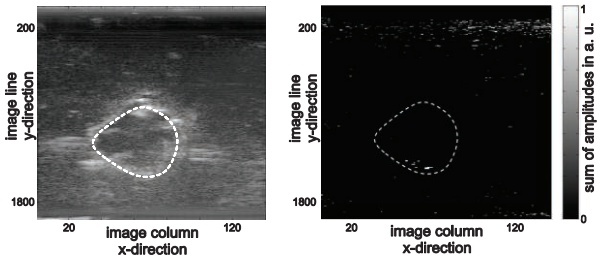


*Fig. 6. Ultrasound B-mode image of silicone bubble containing iron oxide nanoparticles (left) and tissue movement with twice the frequency of the alternating magnetic field using Method B (right). The edge of the bubble is indicated by the dashed line.*

**Method C**

Method C is based on the 1-dimensional cross-correlation. In contrast to Method B only the direction of ultrasonic wave propagation is considered here (y-direction). The advantage in comparison to Method B is a reduced calculation time. Figure 7 illustrates the evaluation algorithm according to Method C. A template of 1 x n elements of the m-th column of the first frame of the RF data is separated. By means of cross-correlation this template is searched in the m-th columns of the other frames. The result is a time-dependent chart of the shift. Just as in Method A and Method B the Fast Fourier Transform is calculated, in which the magnitude values within the frequency band $2f_0 \pm 1$Hz are considered. These values are summed up and can be regarded as an indicator of magnetically induced particle

motion. Figure 8 illustrates the results using the evaluation algorithm according to Method C.

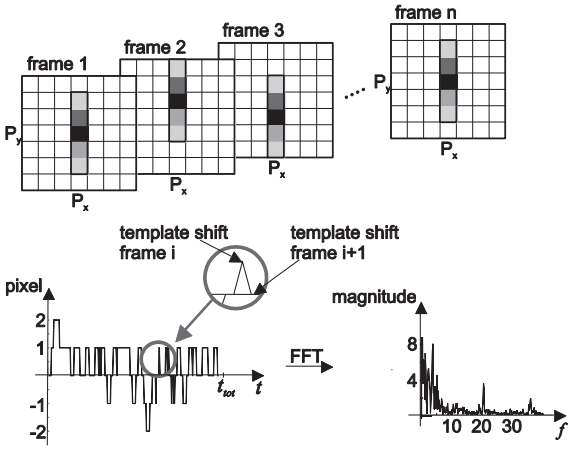


*Fig. 7. Method C: 1D Template Matching (center pixel of template $P_{xy}$ (60, 1600)).*

As discussed before the measuring effect is limited to the bottom of the silicone bubble. As one can see, Method B und Method C yield similar results, which shows that the nanoparticles mainly oscillate in a direction parallel to the direction of ultrasound wave propagation and parallel to the magnetic field gradient, respectively. Like in Method B, the resulting image seems to show tissue movement outside the bubble. However, these signals are located in regions where no reflected signals or only weak reflected signals are visible in the original B-mode image. Consequently those signals also seem to result from noise.

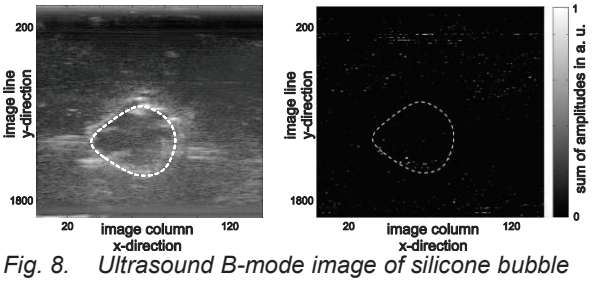


*Fig. 8. Ultrasound B-mode image of silicone bubble containing iron oxide nanoparticles (left) and tissue movement with twice the frequency of the alternating magnetic field using Method C (right). The edge of the bubble is indicated by the dashed line.*

## Results

Three methods were presented by conducting measurements with an experimental setup consisting of a magnet wheel, in order to induce an alternating magnetic field, a phantom containing magnetic nanoparticles and an ultrasound transducer. A 10 mm diameter silicone bubble containing a solution with iron oxide nanoparticles was fixated inside the phantom, which was made of polyvinyl alcohol (PVA). The phantom was placed between the magnet wheel and the ultrasound transducer. The magnet wheel was rotated by a DC motor. The alternating magnetic field with the frequency $f_0$ led to an oscillation of the nanoparticles with the frequency $2f_0$. The received RF data were postprocessed using three different evaluation algorithms. The three implemented methods can detect magnetically excited particle movements. The different algorithms yield similar results, but method A looks most promising. The tissue vibration at the expected frequency reveals the accumulation of nanoparticles at the boundary of the silicone bubble. Because of the weak backscattering of the nanoparticles the content of the bubble cannot be made visible.

## Outlook

The experiments have shown that magnetically excited periodic movements of magnetic nanoparticles cause a measurable effect. It is necessary to clarify by means of further investigations whether the presented technique has practical relevance. Therefore phantoms have to be produced, which behave as realistic as possible. In this work a silicone bubble filled with a nanoparticle solution was used as device under test. In this configuration the particles are able to freely move within the bubble. In the real measuring object the particles are localized in the biological tissue. So the next step will be producing phantoms, in which the particles are stationary distributed and embedded within the tissue mimicking structure. In the case of successful investigations, also measurements applied to real biological tissue perfused by magnetic nanoparticles can be sought. Finally, a suitable combination of the DC magnetic field source (for local particle accumulation) and the AC magnetic field source (for periodic particle movement excitation) has to be established in a later system design.

## References

[1] C. Alexiou, D. Diehl, P. Henninger, H. Iro, R. Röckelein, W. Schmidt, and H. Weber, “A high field gradient magnet for magnetic drug targeting”, *IEEE Trans. Appl. Supercond.* 16, 1527-1530 (2006)

[2] C. Alexiou, R. Tietze, E. Schreiber, R. Jurgons, H. Richter, L. Trahms, H. Rahn, S. Odenbach, and S. Lyer, “Cancer therapy drug loaded magnetic nanoparticles - magnetic drug targeting”, *J. Magnetism Magn. Mater.* 323, 1404-1407 (2011)

[3] J. Oh, M. D. Feldman, J. Kim, C. Condit, S. Emilianov and T. E. Milner, “Detection of magnetic nanoparticles in tissue using magneto-motive ultrasound”, *Nanotechnology*. 17, 4183-4190 (2006)

[4] J. Fromageau, J. Gennisson, C. Schmitt, R. Maurice, R. Mongrain, and G. Cloutier, “Estimation of polyvinyl alcohol cryogel mechanical properties with four ultrasound elastography methods and comparison with gold standard testings”, *IEEE Trans.Ultrasonics, Ferroelectrics, and Frequency Control.* 54, 498-509 (2007)

[5] J. Zaloga, C. Janko, J. Nowak, J. Matuszak, S. Knaup, D. Eberbeck, R. Tietze, H. Unterweger, RP. Friedrich, S. Duerr, R. Heimke-Brinck, E. Baum, I. Cicha, F. Dörje, S. Odenbach, S. Lyer, G. Lee, and C. Alexiou, “Development of a lauric acid/albumin hybrid iron oxide nanoparticle system with improved biocompatibility”, *International Journal of Nanomedicine.* 9, 4847-4866 (2014)

[6] R. Tietze, S. Lyer, S. Dürr, T. Struffert, T. Engelhorn, M. Schwarz, E. Eckert, T. Göen, S. Vasylyev, W. Peukert, F. Wiekhorst, L. Trahms, A. Dörfler, and C. Alexiou, “Efficient drug-delivery using magnetic nanoparticles-biodistribution and therapeutic effects in tumour bearing rabbits”, *Nanomedicine.* 9, 961-971 (2013)

[7] C. Heilmaier, A. Lutz, N. Bolog, D. Weishaupt, B. Seifert, and J. Willmann, “Focal liver lesions: detection and characterization at double-contrast liver MR Imaging with ferucarbotran and gadobutrol versus single-contrast liver MR imaging”, *Radiology*. 253, 724-733 (2009)

[8] M. Harisinghani, M. Saksena, P. Hahn, B. King, J. Kim, M. Torabi, and R. Weissleder, “Ferumoxtran-10-enhanced MR lymphangiography: does contrast-enhanced imaging alone suffice for accurate lymph node characterization?”, *Roentgenol.* 186, 144-148 (2006)

[9] K. Lüdtke-Buzug, J. Haegele, S. Biederer, T. Sattel, M. Erbe, R. Duschka, J. Barkhausen and F. Vogt, “Comparison of commercial iron oxide-based MRI contrast agents with synthesized highperformance MPI tracers”, *Biomed Tech.* 58, 527-533 (2013)